Electronic Supplementary Material (ESI) for Journal of Materials Chemistry A.
This journal is © The Royal Society of Chemistry 2023

Electronic Supporting Information

Atomistic design of two-dimensional covalent organic frameworks with high thermoelectric performance

Tingxia Zhou,[a] Xiaomei Wu,[a] Tianqi Deng,[bc] Haoyuan Li,[d] Zhibin Gao[e] and Wen Shi*[a]

[a.]School of Chemistry, Sun Yat-sen University, Guangzhou, 510006, China. E-mail: shiw59@mail.sysu.edu.cn

[b.]State Key Laboratory of Silicon Materials, School of Materials Science and Engineering, Zhejiang University, Hangzhou, Zhejiang, 310027, China

[c.]Institute of Advanced Semiconductors & Zhejiang Provincial Key Laboratory of Power Semiconductor Materials and Devices, ZJU-Hangzhou Global Scientific and Technological Innovation Center, Hangzhou, Zhejiang, 311200, China

[d.]School of Microelectronics, Shanghai University, Shanghai, 201800, China

[e.]State Key Laboratory for Mechanical Behavior of Materials, Xi'an Jiaotong University, Xi'an, Shaanxi, 710049, China

Table of Contents

Section 1. Computational details

Model setup and structural optimizations. The monolayer structural models of our studied 17 two-dimensional COFs are shown in Fig. S1. Both the lattice constants (*i.e.*, *a* and *b*) and atomic positions were optimized by using the projector augmented-wave (PAW) method[1] with Perdew-Burke-Ernzerhof (PBE) exchange-correlation functional[2] including the Grimme's D3 dispersion correction[3] in Vienna *Ab initio* Simulation Package (VASP)[4] (version 6.2.1). The Γ *k*-point of 4×4×1 was used for **1**, **4**, **10**, and **12**–**13**, and the Γ *k*-point of 2×2×1 was used for **2**–**3**, **5**–**9**, **10**, and **14**–**17** during the structural optimization. The cutoff energy for the plane-wave basis set is 500 eV. The convergence criterion for the total energy was set to be 10^{-5} eV, and the residual force on each atom should be smaller than 0.01 eV $Å^{-1}$.

For the single-point energy and charge density calculations, the Γ *k*-point of 6×6×1 was used for **1**, **4**, **10**, and **12**–**13**, and the Γ *k*-point of 4×4×1 was used for **2**–**3**, **5**–**9**, **10**, and **14**–**17**. Moreover, the cutoff energy for the plane-wave basis set is 600 eV. The convergence criterion for the total energy was set to be 10^{-6} eV. The relationship between the calculated total energy and lattice parameters of our studied 17 COFs are shown in Fig. S2.

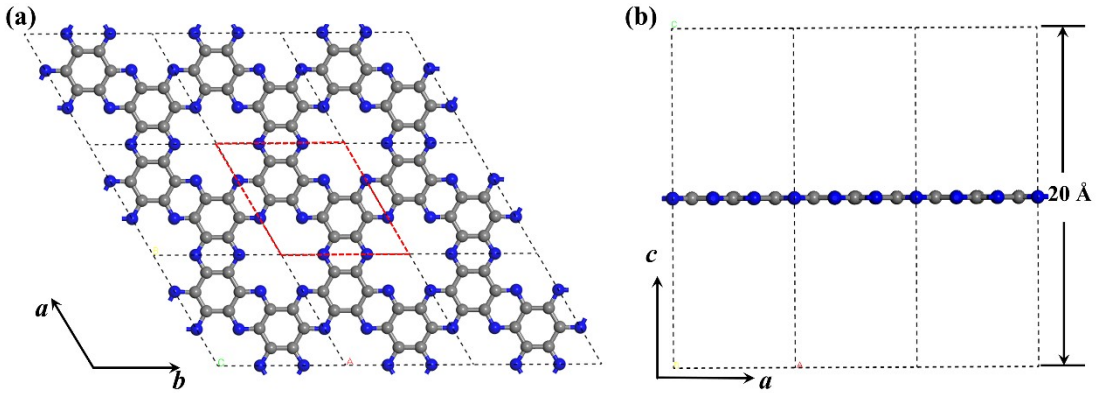

Fig. S1 Schematic diagram of the model of single-layer two-dimensional COFs viewed in the (**a**) *ab* plane and (**b**) *ac* plane. The black dashed lines stand for the crystal lattices. The red dashed line shows the unit cell.

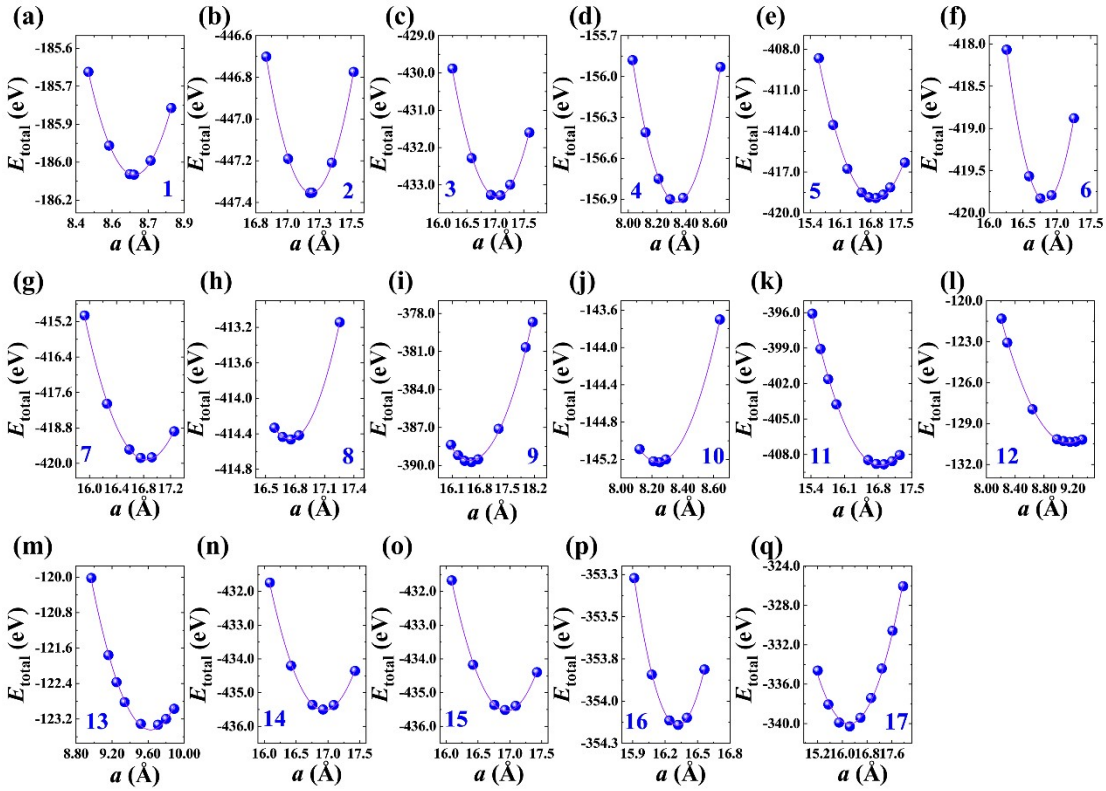

Fig. S2 Relationship between the calculated total energy and lattice parameters of our studied 17 COFs. The violet lines show the trend.

Electronic structure calculations. To better understand the TE transport processes of our studied 17 two-dimensional COFs, their band structures were computed along the high-symmetry line. Furthermore, their hole effective masses (m^*) were achieved by the formula, $1/m^* = \partial^2 E/(\hbar^2 \partial k^2)$, where, $\hbar$ is the reduced Planck's constant; E and k are the band energy and the electron wave vector, respectively.

Boltzmann transport equation for TE performance calculations. In order to avoid the interlayer interaction, the unit cell lengths along the *c* axis were fixed at 20 Å. On the basis of the published experimental works, it is reported that the interlayer distances of the COF-based materials fall in the range of 3.2–4.1 Å (Table S1). Therefore, we used 3.5 Å as the interlayer distance of our studied COFs to calculate their hole concentrations, conductivities, and TE power factors.

Table S1. Conclusion of the experimentally reported interlayer distance (l_{layer}) of

COF-based materials at room temperature.

	l_{layer} (Å)	Ref.
QA-COF	3.2	[5]
ABBPM-COF	3.3	[6]
CS-COF	4.01	[7]
C2P-5	3.45	[8]
C_5N	3.40	[9]
C_2N-*h*2D	3.28	[10]
COF-316	3.163	[11]
JUC-505	3.4624	[12]
JUC-506	3.5704	[12]
EB-COF	3.3	[13]
PD-COF	3.4	[13]
DAAQ-COF	3.6	[13]
TAP-COF	3.5	[13]

Deformation potential (DP) theory for lattice vibration scattering. The vacuum energy level calibration method[14,15] was utilized to calculate the absolute energy level of valence band maximum (Fig. S3). The electrostatic potential profiles along the crystal axis *c* direction were calculated by the offsets between the band edge positions and vacuum level, namely, $E_{VBM} = E_{VBM}^{0} - E_{vacuum}$, where E_{VBM}^{0} is the uncalibrated energy level of valence band maximum, and E_{vacuum} is the vacuum level.

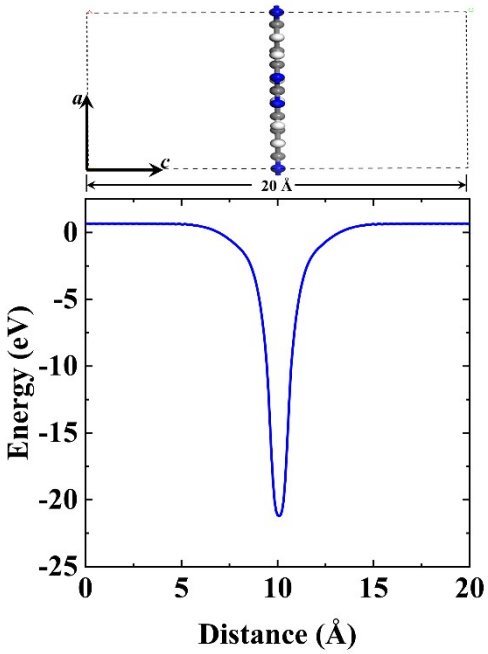

Fig. S3 Schematic diagram of vacuum energy level calibration method.[14,15] The electrostatic potential distribution for **5** along the crystal axis *c* direction is taken as an example to show in this figure.

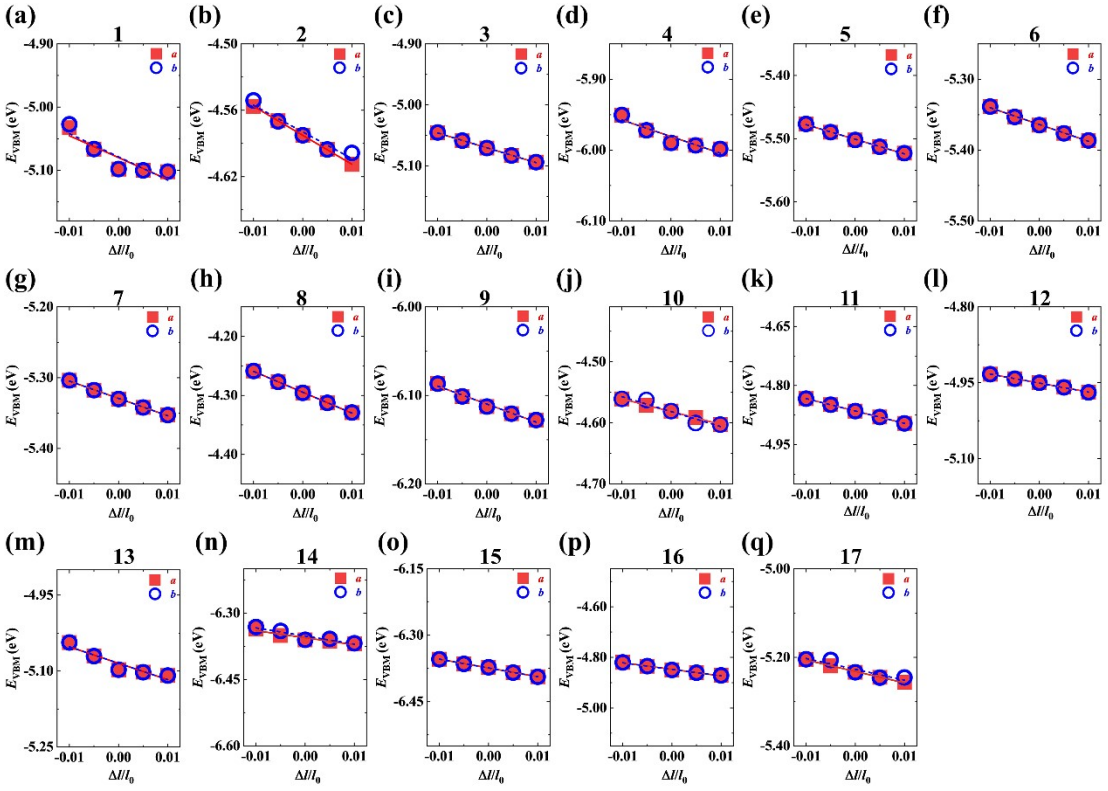

Fig. S4 The valence band maximum (E_{VBM}) shifts with respect to the dilations ($\Delta l/l_0$) for our studied 17 two-dimensional COFs along the *a* (red square) and *b* (blue circle)

directions, respectively. The solid and short-dashed lines are the linearly fitted lines for the *a* and *b* directions, respectively.

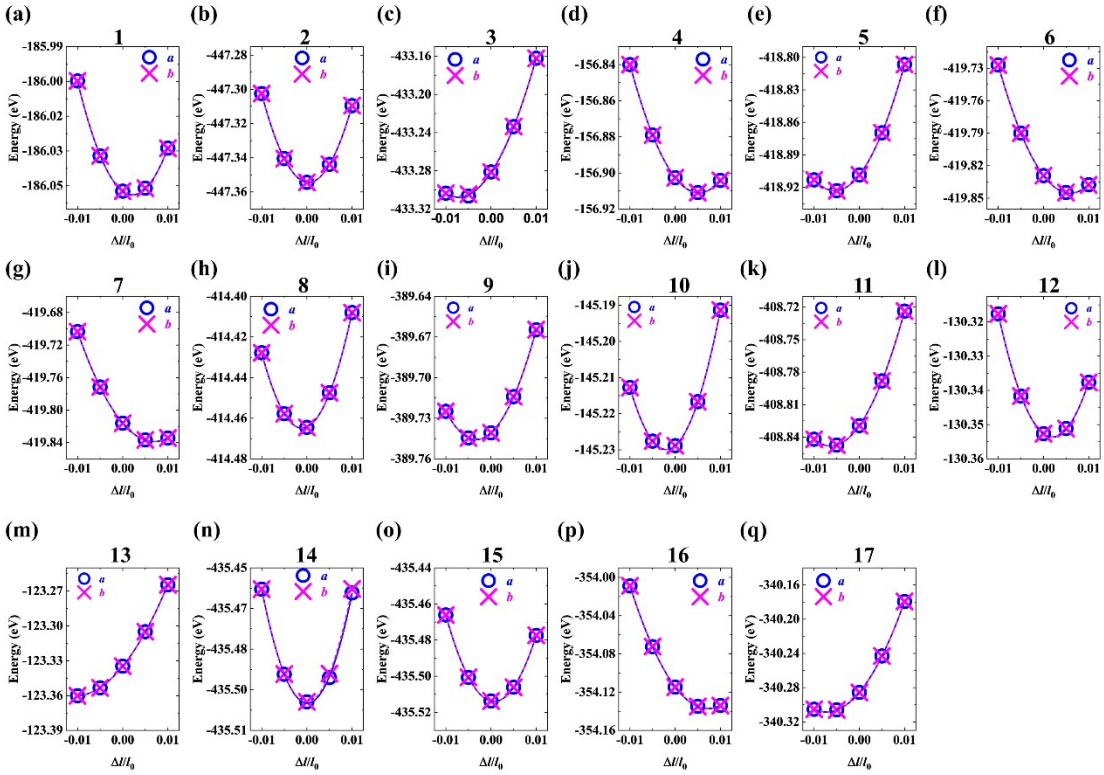

Fig. S5 The total energy with respect to dilations ($^{\Delta l/l_0}$) for our studied 17 two-dimensional COFs along the crystal axis *a* (blue circle) and *b* (magenta cross) directions, respectively. The blue solid and magenta short-dashed lines are the fitted lines along the *a* and *b* directions, respectively.

Section 2. Geometric structure of two-dimensional COFs

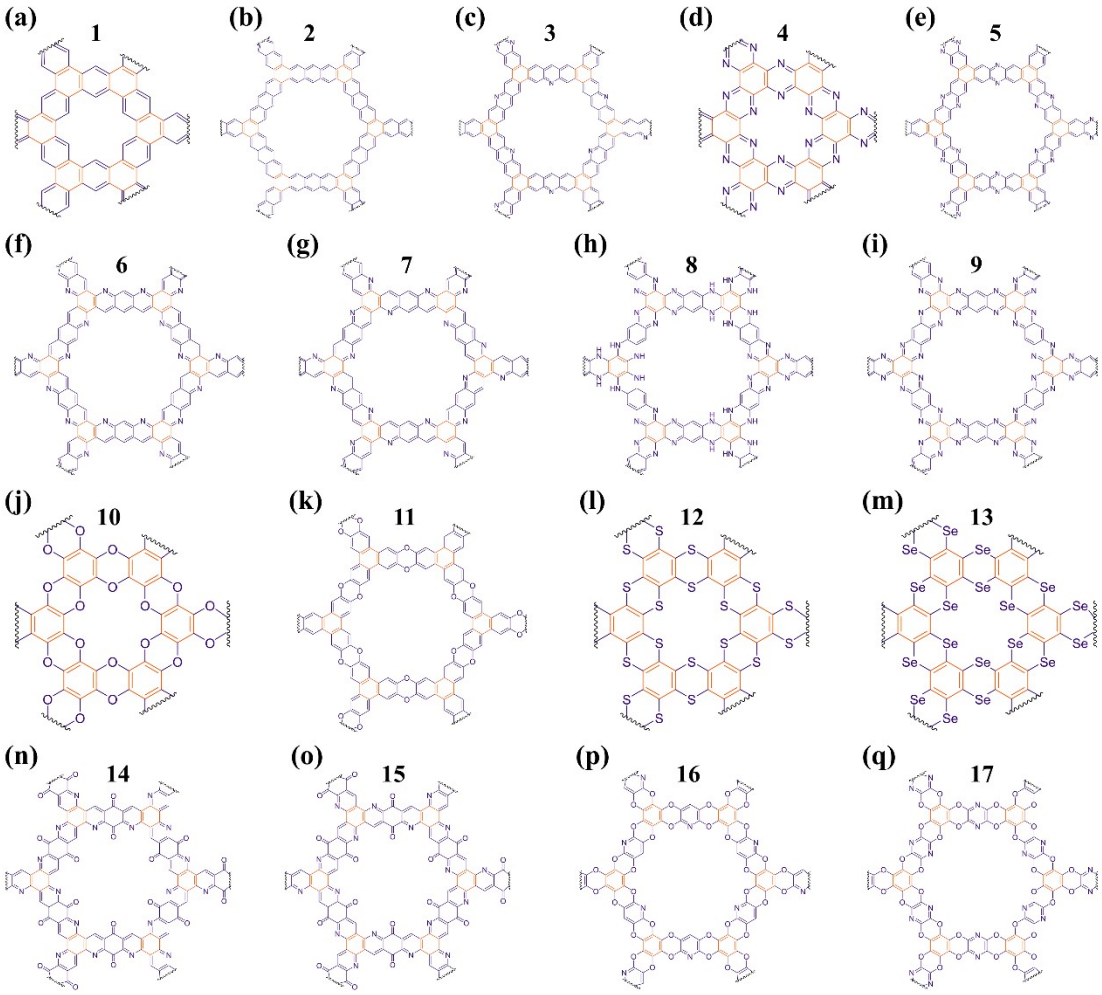

Fig. S6 Chemical structures of our studied 17 two-dimensional COFs with fused ring structures. The linker and knot parts are displayed in purple and orange, respectively.

Table S2. Optimized lattice parameters and pore diameters of our studied 17 two-dimensional COFs. $a = b$, $\alpha = \beta = 90^{0}$, and $\gamma = 120^{0}$. The vacuum layer along the c axis is set to be 20 Å.

	a (Å)	Pore diameter (Å)
1	8.62	8.62
2	17.2	17.2
3	17.1	17.1
4	8.29	8.29
5	16.9	16.9
6	16.8	16.8
7	16.8	16.8
8	16.8	16.8
9	16.6	16.6

10	8.25	8.25
11	16.9	16.9
12	9.16	9.16
13	9.71	9.71
14	16.9	16.9
15	16.9	16.9
16	16.2	16.2
17	16.2	16.2

Section 3. Descriptions of electronic structure

Table S3. Computed contributions of the knot and linker parts to the valence band, bandgap (E_g) and valence band width (W_{VB}) of our studied 17 two-dimensional COFs.

	Knot part (%)	Linker part (%)	E_g (eV)	W_{VB} (meV)
1	60.4	39.6	1.78	1.05×10^3
2	48.3	51.7	0.917	390
3	47.0	53.0	1.01	343
4	15.7	84.3	1.65	124
5	45.7	54.3	0.944	330
6	41.0	59.0	1.18	245
7	40.2	59.8	1.12	277
8	43.1	56.9	1.18	262
9	33.6	66.4	1.04	228
10	29.5	70.5	2.23	852
11	50.0	50.0	2.34	187
12	25.0	75.0	1.75	403
13	19.8	80.2	1.37	176
14	3.60	96.4	1.64	25.0
15	5.20	94.8	1.65	76.5
16	36.0	64.0	2.59	103
17	35.5	64.5	2.30	96.2

Table S4. Hole effective mass (m_h^*/m_e) and geometric mean hole effective mass of our studied 17 two-dimensional COFs. The reciprocal coordinates of high-symmetry *k*-points in the first Brillouin zone are Γ = (0, 0, 0), M = (1/2, 0, 0), and K = (1/3, 1/3, 0).

		m_h^*/m_e		Mean m_h^*/m_e
1	Γ-M	M -K	Γ-K	0.397

	0.720	0.192	0.451	
2	Γ-M 0.497	M -K 0.229	Γ-K 0.964	0.479
3	Γ-M 0.569	M -K 0.213	Γ-K 0.778	0.455
4	Γ-M 3.95	M -K 8.90	Γ-K 3.42	4.93
5	Γ-M 0.657	M -K 0.197	Γ-K 0.651	0.438
6	Γ-M 1.28	M -K 0.238	Γ-K 0.660	0.586
7	Γ-M 0.796	M -K 0.231	Γ-K 0.663	0.496
8	M -Γ 0.439	K-M 0.546	K -Γ 0.448	0.475
9	Γ-M 1.96	M -K 0.233	Γ-K 0.623	0.658
10	M -Γ 0.630	K-M 0.817	K -Γ 0.670	0.702
11	M -Γ 0.656	K-M 0.781	K -Γ 0.686	0.706
12	M -Γ 0.928	K-M 6.32	K -Γ 1.54	2.08
13	M -Γ 1.93	M -K 5.03	K -Γ 3.20	3.15
14	Γ-M 5.82	M -K 7.81	Γ-K 7.88	7.10
15	Γ-M 5.72	M -K 4.42	K -Γ 11.49	6.62
16	Γ-M 1.50	M -K 0.94	Γ-K 1.44	1.26
17	Γ-M 1.69	M -K 0.99	Γ-K 1.63	1.40

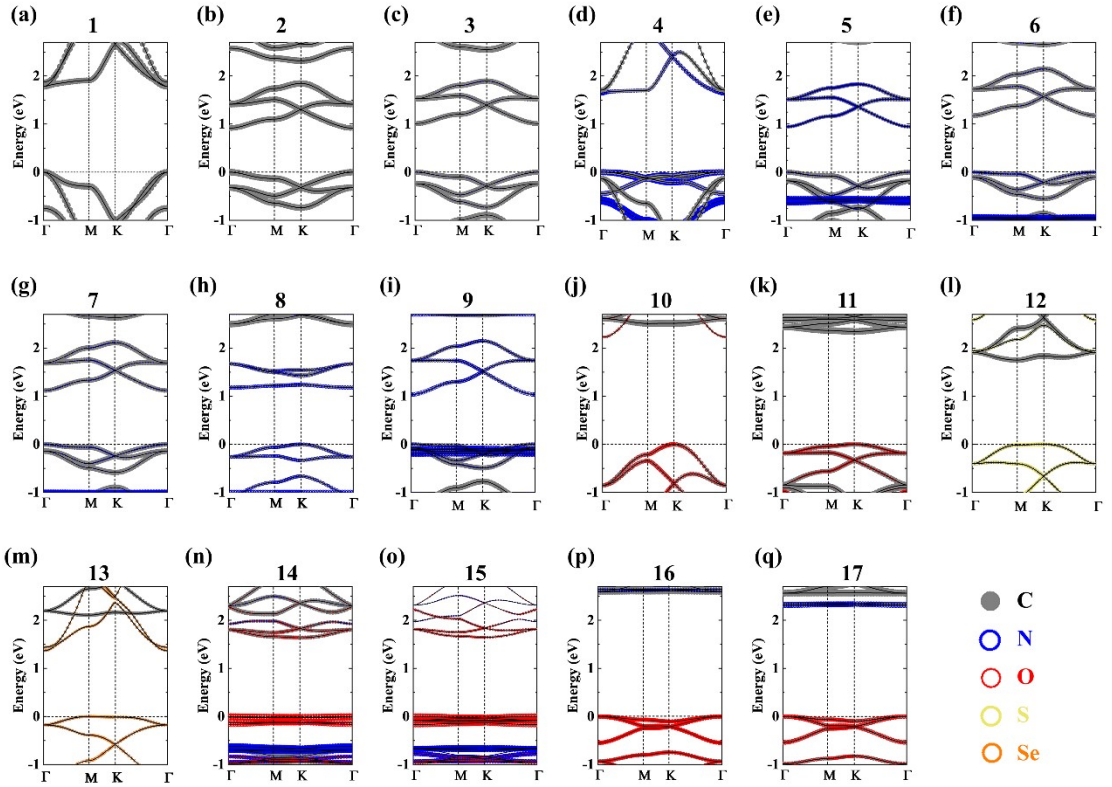

Fig. S7 Element-projected band structures of our studied 17 two-dimensional COFs. The symbol size denotes the relative weight of the component ratio. The carbon, nitrogen, oxygen, sulfur, and selenium element contributions are displayed in grey, blue, red, yellow, and orange, respectively. The non-projected band structures are shown in black solid lines. The Fermi energy levels are displayed in black horizontal dashed lines. The reciprocal coordinates of high-symmetry *k*-points in the first Brillouin zone are Γ = (0, 0, 0), M = (1/2, 0, 0), and K = (1/3, 1/3, 0).

Table S5. Contributions of different elements to the valence band of our studied 17 two-dimensional COFs.

	C (%)	N (%)	O (%)	S (%)	Se (%)	H (%)
1	99.3	–	–	–	–	0.717
2	99.2	–	–	–	–	0.820
3	84.1	15.6	–	–	–	0.339
4	33.5	66.5	–	–	–	–
5	78.6	21.0	–	–	–	0.427
6	73.9	25.4	–	–	–	0.689
7	76.2	23.1	–	–	–	0.701
8	55.1	43.9	–	–	–	1.02

9	66.4	32.8	–	–	–	0.748
10	49.6	–	50.4	–	–	–
11	62.8	–	37.2	–	–	0.000
12	46.4	–	—	53.6	–	–
13	40.2	–	–	–	59.8	–
14	23.1	5.72	70.9	–	–	0.314
15	21.9	10.2	67.8	–	–	0.105
16	46.5	0.448	53.0	–	–	0.000
17	46.4	0.686	52.9	–	–	–

Table S6. The energy levels of valence band maximum (E_{VBM}) of our studied 17 two-dimensional COFs. The highest occupied molecular orbital (HOMO) energy levels (E_{HOMO}) of the isolated linker parts are also shown in the table. The knot part of all materials can be regarded as a benzene ring, and its HOMO energy level is –7.00 eV.

	E_{VBM} (eV)	Linker part
		E_{HOMO} (eV)
1	−5.10	−7.00
2	–4.58	–5.50
3	–5.07	–5.97
4	–5.99	–7.16
5	–5.50	–6.39
6	–5.36	–6.18
7	–5.33	–6.05
8	–4.30	–4.68
9	–6.11	–6.82
10	–4.58	–5.35
11	–4.86	–5.53
12	–4.95	–3.31
13	–5.10	–5.05
14	–6.36	–7.29
15	–6.37	–7.35
16	–4.85	–5.39
17	–5.23	–5.61

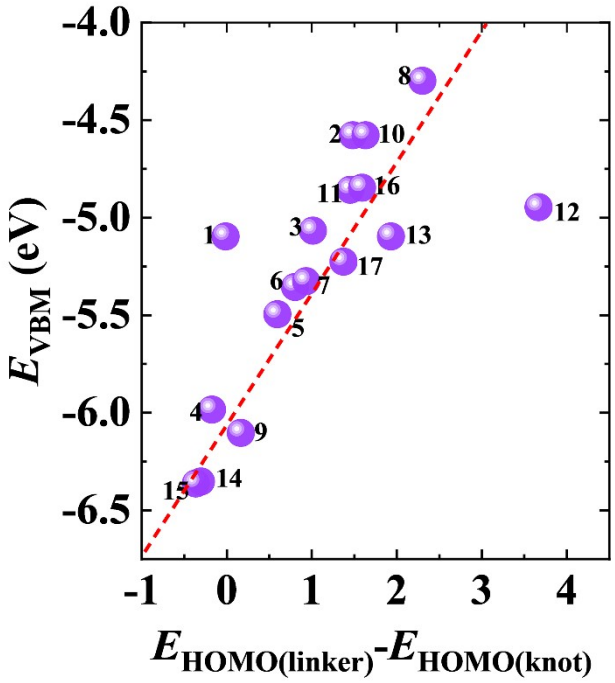

Fig. S8 Relationship between the energy level of valence band maximum (E_{VBM}), and the energy-level difference between the HOMO of the isolated linker and knot parts ($E_{HOMO(linker)} - E_{HOMO(knot)}$) for our studied 17 two-dimensional COFs. The red dashed line displays the trend.

Section 4. Quantitative descriptions of interaction of charge carriers with lattice vibrations

Table S7. Hole DP constants (E_1) and elastic constants (C_{ii}) along the *a* and *b* directions, respectively for our studied 17 two-dimensional COFs.

	Directions	E_1 (eV)	C_{ii} (J m^{-2})
1	*a*	3.46	328
	b	3.67	328
2	*a*	2.62	121
	b	2.41	121
3	*a*	2.42	124
	b	2.43	122
4	*a*	2.34	328
	b	2.35	328
5	*a*	2.31	126
	b	2.31	126

6	*a*	2.37	123
	b	2.37	123
7	*a*	2.45	124
	b	2.45	124
8	*a*	3.54	122
	b	3.53	122
9	*a*	2.03	124
	b	2.03	124
10	*a*	2.08	291
	b	2.44	291
11	*a*	3.14	120
	b	3.14	120
12	*a*	1.77	221
	b	1.78	221
13	*a*	3.24	175
	b	3.25	176
14	*a*	1.59	107
	b	1.83	108
15	*a*	1.98	109
	b	1.98	109
16	*a*	2.59	121
	b	2.58	121
17	*a*	2.59	121
	b	2.45	121

Table S8. The hole relaxation time ($\langle\tau\rangle$), hole mean free path (l), and hole mobility (μ) along the *a* and *b* directions, respectively for our studied 17 two-dimensional COFs.

	$\langle\tau\rangle$ (fs)	l (Å)		μ (cm^2 V^{-1} s^{-1})	
		a	*b*	*a*	*b*
1	95.5	1.51×10^3	1.44×10^3	1.45×10^3	1.43×10^3
2	48.9	380	376	3.15×10^3	3.12×10^3
3	4.71	31.4	31.6	49.1	48.1
4	2.95	5.33	5.35	0.502	0.502
5	296	2.10×10^3	2.08×10^3	5.35×10^3	4.92×10^3
6	232	1.27×10^3	1.28×10^3	694	676
7	254	1.49×10^3	1.50×10^3	1.55×10^3	1.52×10^3
8	159	1.11×10^3	1.06×10^3	264	263
9	190	615	599	397	397
10	836	9.42×10^3	9.30×10^3	1.22×10^3	1.22×10^3

11	203	1.17×10^{3}	1.14×10^{3}	358	148
12	534	3.76×10^{3}	3.78×10^{3}	159	159
13	48.6	154	157	11.1	11.1
14	29.5	13.2	13.5	1.26	1.24
15	6.97	5.29	5.20	0.558	0.548
16	53.5	128	127	256	271
17	42.8	97.0	97.2	57.4	59.6

Section 5. First-principles predictions of TE transport properties

Table S9. Summary of the experimentally reported hole concentration (N) of some representative COFs at room temperature. Here, we study the TE properties of 17 two-dimensional COFs at the hole concentration of 10^{13}–10^{15} cm^{-3}.

	N (cm^{-3})	Ref.
ZnPc-pz	9.12×10^{11} 8.81×10^{13}	16,17
CuPc-pz	2.09×10^{12} 8.93×10^{13}	16,17
NiPc-CoTAA	2.14×10^{13}	18
PyVg-COF	1.25×10^{12}	19
2DPI	1.45×10^{17}	20
HHTP-MIDA-COF CuPc-MIDA-COF	4.5×10^{11} 2.6×10^{12}	21
BUCT-COF-1	$(3.40\pm0.40)\times10^{10}$	22
BUCT-COF-4	$(1.81\pm0.05)\times10^{11}$ $(6.63\pm0.03)\times10^{12}$	23
C2P-5	$(2.73\pm5.58)\times10^{18}$	8
AntTTH	2.38×10^{12} 7.50×10^{12}	24
C_5N	8.98×10^{16}	9

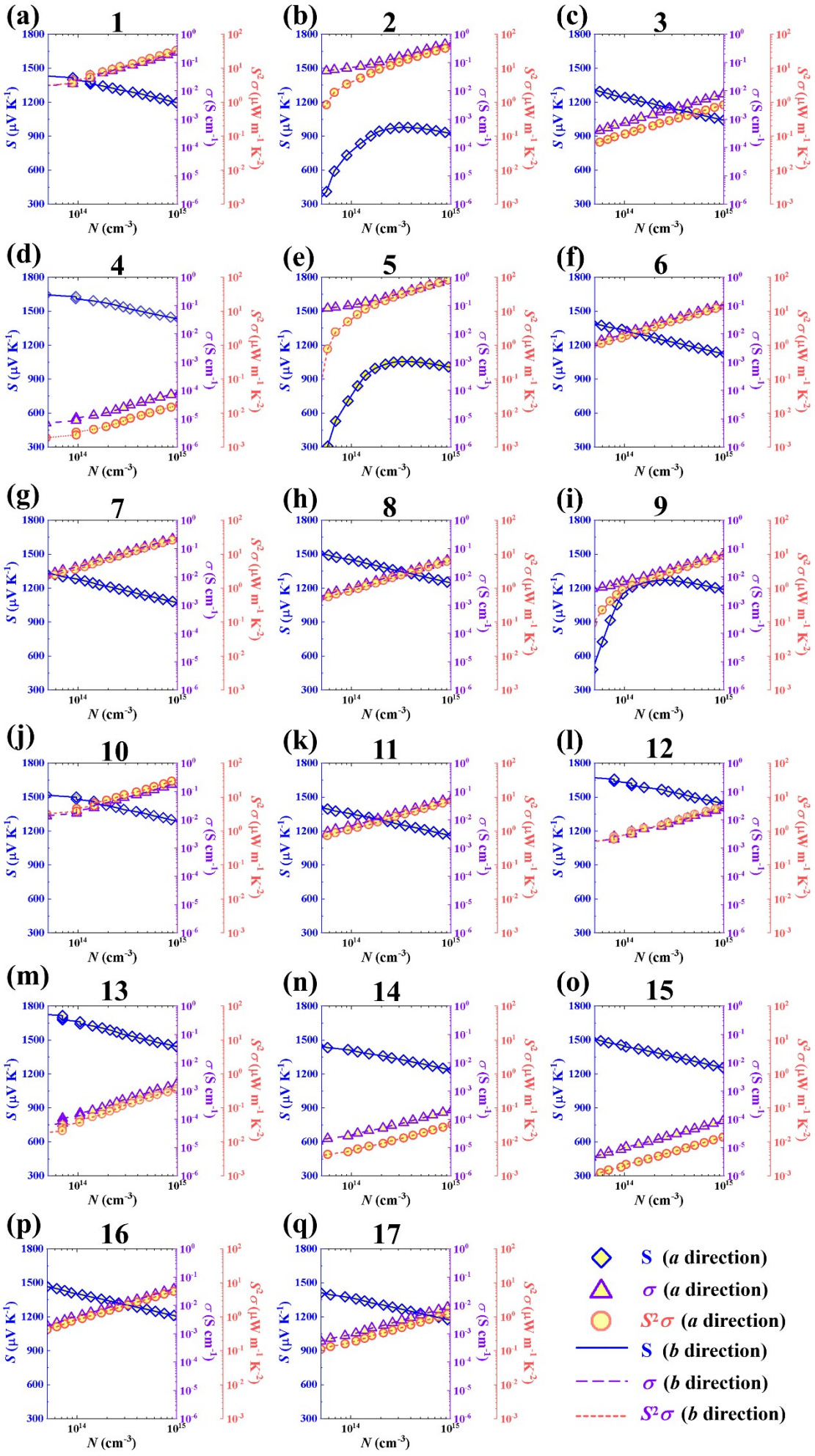
(a) 1
(b) 2
(c) 3
(d) 4
(e) 5
(f) 6
(g) 7
(h) 8
(i) 9
(j) 10
(k) 11
(l) 12
(m) 13
(n) 14
(o) 15
(p) 16
(q) 17
S (μV K-1)
σ (S cm-1)
S2σ (μW m-1 K-2)
N (cm-3)
S (a direction)
σ (a direction)
S2σ (a direction)
S (b direction)
σ (b direction)
S2σ (b direction)

Fig. S9 Seebeck coefficient (S), conductivity (σ), and power factor ($S^2\sigma$) of our studied 17 two-dimensional COFs along the *a* and *b* directions, respectively at the hole concentration from 5×10^{13} cm^{-3} to 10^{15} cm^{-3} at room temperature. The Seebeck coefficients are displayed in blue diamond and blue solid line along the *a* and *b* directions, respectively. The conductivities are displayed in purple triangle and purple dashed line along the *a* and *b* directions, respectively. The power factors are displayed in orange circle and orange short dashed line along the *a* and *b* directions, respectively.

Table S10. Seebeck coefficient (S), conductivity (σ), and power factor ($S^2\sigma$) for our studied 17 two-dimensional COFs along the *a* and *b* directions at the hole concentration (N) of around 5×10^{13}, 10^{14}, 5×10^{14}, and 10^{15} cm^{-3}, respectively at room temperature.

	N (cm^{-3})	S (μV K^{-1})		σ (S cm^{-1})		$S^2\sigma$ (μW m^{-1} K^{-2})	
		a	*b*	*a*	*b*	*a*	*b*
1	4.44×10^{13}	1.43×10^{3}	1.44×10^{3}	0.0147	0.0145	3.02	2.99
	1.33×10^{14}	1.38×10^{3}	1.38×10^{3}	0.0277	0.0274	5.28	5.22
	5.32×10^{14}	1.25×10^{3}	1.25×10^{3}	0.122	0.121	19.1	18.9
	1.24×10^{15}	1.18×10^{3}	1.18×10^{3}	0.285	0.282	39.6	39.2
2	5.59×10^{13}	410	408	0.0505	0.0501	0.848	0.834
	1.02×10^{14}	1.24×10^{3}	1.24×10^{3}	7.53×10^{-4}	7.36×10^{-4}	0.116	0.114
	4.58×10^{14}	971	972	0.237	0.235	22.4	22.2
	1.08×10^{15}	918	918	0.549	0.544	46.2	45.8
3	4.52×10^{13}	1.31×10^{3}	1.31×10^{3}	3.23×10^{-4}	3.16×10^{-4}	0.0556	0.0545
	1.02×10^{14}	1.24×10^{3}	1.24×10^{3}	7.53×10^{-4}	7.36×10^{-4}	0.116	0.114
	5.31×10^{14}	1.10×10^{3}	1.10×10^{3}	4.10×10^{-3}	4.01×10^{-3}	0.49	0.48
	1.22×10^{15}	1.02×10^{3}	1.02×10^{3}	9.57×10^{-3}	9.37×10^{-3}	1.00	0.982
4	4.80×10^{13}	1.67×10^{3}	1.67×10^{3}	5.63×10^{-6}	5.62×10^{-6}	1.56×10^{-3}	1.56×10^{-3}
	1.44×10^{14}	1.59×10^{3}	1.59×10^{3}	1.31×10^{-5}	1.31×10^{-5}	3.32×10^{-3}	3.32×10^{-3}
	5.28×10^{14}	1.48×10^{3}	1.48×10^{3}	4.69×10^{-5}	4.68×10^{-5}	0.0103	0.0103
	1.34×10^{15}	1.41×10^{3}	1.41×10^{3}	1.09×10^{-4}	1.09×10^{-4}	0.0217	0.0217
5	5.76×10^{13}	308	300	0.0797	0.0737	0.757	0.664
	1.15×10^{14}	840	837	0.112	0.103	7.88	7.21
	4.95×10^{14}	1.05×10^{3}	1.05×10^{3}	0.429	0.394	47.1	43.4

	1.16×10^{15}	991	994	0.995	0.915	97.8	90.3
6	4.70×10^{13}	1.39×10^{3}	1.40×10^{3}	4.75×10^{-3}	4.62×10^{-3}	0.922	0.901
	1.06×10^{14}	1.32×10^{3}	1.32×10^{3}	0.0111	0.0108	1.93	1.89
	5.52×10^{14}	1.18×10^{3}	1.18×10^{3}	0.0604	0.0588	8.33	8.14
	1.03×10^{15}	1.12×10^{3}	1.12×10^{3}	0.114	0.111	14.3	14.0
7	4.70×10^{13}	1.34×10^{3}	1.34×10^{3}	0.0113	0.0111	2.02	1.99
	1.17×10^{14}	1.27×10^{3}	1.27×10^{3}	0.0264	0.0259	4.21	4.15
	4.70×10^{14}	1.14×10^{3}	1.14×10^{3}	0.116	0.114	15.0	14.8
	1.10×10^{15}	1.06×10^{3}	1.07×10^{3}	0.271	0.267	30.7	30.2
8	4.70×10^{13}	1.51×10^{3}	1.51×10^{3}	1.98×10^{-3}	1.98×10^{-3}	0.451	0.450
	1.17×10^{14}	1.44×10^{3}	1.44×10^{3}	4.62×10^{-3}	4.62×10^{-3}	0.954	0.952
	4.82×10^{14}	1.31×10^{3}	1.31×10^{3}	0.0204	0.0204	3.49	3.48
	1.13×10^{15}	1.24×10^{3}	1.24×10^{3}	0.0476	0.0475	7.26	7.25
9	5.99×10^{13}	725	666	4.24×10^{-3}	4.34×10^{-3}	0.223	0.192
	1.20×10^{14}	1.21×10^{3}	1.19×10^{3}	8.08×10^{-3}	8.13×10^{-3}	1.18	1.15
	5.39×10^{14}	1.24×10^{3}	1.23×10^{3}	0.0339	0.0339	5.18	5.13
	1.01×10^{15}	1.19×10^{3}	1.18×10^{3}	0.0640	0.0640	9.01	8.93
10	4.85×10^{13}	1.57×10^{3}	1.57×10^{3}	7.32×10^{-3}	7.32×10^{-3}	1.81	1.81
	1.45×10^{14}	1.46×10^{3}	1.46×10^{3}	0.0261	0.0261	5.58	5.58
	4.85×10^{14}	1.35×10^{3}	1.35×10^{3}	0.0931	0.0931	17.0	17.0
	1.12×10^{15}	1.28×10^{3}	1.28×10^{3}	0.217	0.217	35.6	35.6
11	4.61×10^{13}	1.41×10^{3}	1.48×10^{3}	3.03×10^{-3}	1.25×10^{-3}	0.605	0.272
	1.15×10^{14}	1.34×10^{3}	1.40×10^{3}	7.07×10^{-3}	2.92×10^{-3}	1.27	0.573
	5.41×10^{14}	1.21×10^{3}	1.27×10^{3}	0.0312	0.0129	4.58	2.09
	1.03×10^{15}	1.16×10^{3}	1.22×10^{3}	0.0589	0.0243	7.89	3.61
12	3.94×10^{13}	1.68×10^{3}	1.68×10^{3}	1.66×10^{-3}	1.66×10^{-3}	0.468	0.468
	1.18×10^{14}	1.62×10^{3}	1.62×10^{3}	3.14×10^{-3}	3.14×10^{-3}	0.827	0.827
	5.12×10^{14}	1.49×10^{3}	1.49×10^{3}	0.0139	0.0139	3.09	3.09
	1.02×10^{15}	1.44×10^{3}	1.44×10^{3}	0.0262	0.0262	5.42	5.42
13	3.50×10^{13}	1.73×10^{3}	1.73×10^{3}	5.72×10^{-5}	5.73×10^{-5}	0.0172	0.0172
	1.05×10^{14}	1.66×10^{3}	1.66×10^{3}	1.33×10^{-4}	1.34×10^{-4}	0.0368	0.0369
	5.25×10^{14}	1.50×10^{3}	1.50×10^{3}	8.99×10^{-4}	9.00×10^{-4}	0.201	0.202
	1.19×10^{15}	1.42×10^{3}	1.42×10^{3}	2.10×10^{-3}	2.10×10^{-3}	0.425	0.426
14	4.61×10^{13}	1.45×10^{3}	1.45×10^{3}	1.70×10^{-5}	1.67×10^{-5}	3.57×10^{-3}	3.53×10^{-3}
	1.15×10^{14}	1.40×10^{3}	1.40×10^{3}	3.20×10^{-5}	3.16×10^{-5}	6.25×10^{-3}	6.17×10^{-3}
	5.30×10^{14}	1.29×10^{3}	1.29×10^{3}	1.14×10^{-4}	1.13×10^{-4}	0.0189	0.0187

	1.03×10^{15}	1.23×10^{3}	1.23×10^{3}	2.16×10^{-4}	2.13×10^{-4}	0.0328	0.0323
15	4.61×10^{13}	1.51×10^{3}	1.51×10^{3}	4.52×10^{-6}	4.44×10^{-6}	1.03×10^{-3}	1.02×10^{-3}
	1.04×10^{14}	1.44×10^{3}	1.44×10^{3}	1.05×10^{-5}	1.04×10^{-5}	2.19×10^{-3}	2.15×10^{-3}
	5.07×10^{14}	1.31×10^{3}	1.31×10^{3}	4.65×10^{-5}	4.57×10^{-5}	8.00×10^{-3}	7.86×10^{-3}
	1.21×10^{15}	1.24×10^{3}	1.24×10^{3}	1.09×10^{-4}	1.07×10^{-4}	0.0167	0.0164
16	5.00×10^{13}	1.47×10^{3}	1.46×10^{3}	1.97×10^{-3}	2.08×10^{-3}	0.424	0.445
	1.13×10^{14}	1.39×10^{3}	1.39×10^{3}	4.60×10^{-3}	4.86×10^{-3}	0.893	0.938
	5.00×10^{14}	1.27×10^{3}	1.26×10^{3}	0.0203	0.0214	3.25	3.41
	1.15×10^{15}	1.19×10^{3}	1.19×10^{3}	0.0473	0.0500	6.73	7.07
17	5.00×10^{13}	1.41×10^{3}	1.41×10^{3}	5.55×10^{-4}	5.77×10^{-4}	0.111	0.114
	1.13×10^{14}	1.36×10^{3}	1.35×10^{3}	1.05×10^{-3}	1.09×10^{-3}	0.193	0.200
	5.00×10^{14}	1.23×10^{3}	1.23×10^{3}	4.62×10^{-3}	4.80×10^{-3}	0.699	0.722
	1.16×10^{15}	1.16×10^{3}	1.15×10^{3}	0.0108	0.0112	1.44	1.49

Table S11. Summary of the experimentally reported hole conductivity (σ), mobility (μ), Seebeck coefficient (S), and power factor ($S^2\sigma$) of some representative COFs at room temperature.

	μ ($cm^2\ V^{-1}\ s^{-1}$)	S ($\mu V\ K^{-1}$)	σ ($S\ cm^{-1}$)	$S^2\sigma$ ($\mu W\ m^{-1}\ K^{-2}$)	Ref.
FL-COF-1	–	2.45×10^{3}	1.0×10^{-4}	0.063	25
	–	1.75×10^{3}	1.75×10^{-4}	0.0526	
	–	3.23×10^{3}	3.34×10^{-5}	0.0362	
TANG-COF	–	–	1.6×10^{-5} 1.5×10^{-3} 5×10^{-12} 2×10^{-3}	–	26
CS-COF	4.2	–	–	–	7
2DPI	4.3×10^{-3}	–	1×10^{-4}	–	20
WTA	–	–	3.78×10^{-6} 7.35×10^{-5}	–	27
BUCT-COF-4	1.97±0.06 2.62±0.03	–	5.75×10^{-6} 2.79×10^{-4}	–	23
C_2N-*h*2D	13.5 20.6	–	–	–	10
C2P-5	1.96−4.0	–	1.75	–	8
C_5N	501	–	7.2	–	9
HP-FAN	1.42 1.49	–	3.8×10^{-2}	–	28

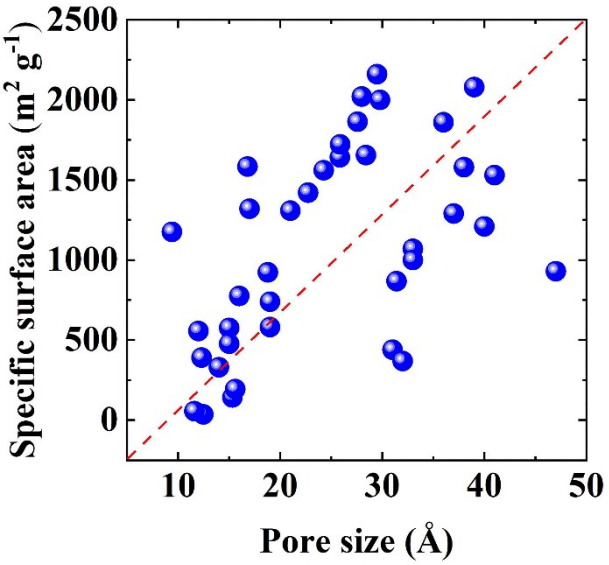

Fig. S10 Relationship between the experimentally reported specific surface area and pore size for COFs with hexagonal topological structures. The red dashed line displays the trend. The detailed data and sources are given in the Table S12.

Table S12. Summary of the experimentally reported specific surface area and pore size for some representative COFs with hexagonal topological structure.

	Specific surface area (m^2 g^{-1})	Pore size (Å)	Ref.
2D DA-COF	2021	28	[29]
ACOF-1	1176	9.4	[30]
100%N3-COF-5	1421	22.74	[31]
75%N3-COF-5	1641	25.85	[31]
50%N3-COF-5	1722	25.87	[31]
25%N3-COF-5	1864	27.57	[31]
5%N3-COF-5	2160	29.49	[31]
100%AcTrz-COF-5	36	12.48	[31]
75%AcTrz-COF-5	142	15.32	[31]
50%AcTrz-COF-5	194	15.6	[31]
25%AcTrz-COF-5	1561	24.26	[31]
5%AcTrz-COF-5	2000	29.78	[31]
HHTP-DPB COF	930	47	[32]
TA	1070	33	[33]
Pyrene-2,7	1210	40	[33]
TT	1860	36	[33]
BDT	1530	41	[33]
BDT-OMe	2080	39	[33]

BDT-OEt	1580	38	33
BDT-OPr	1290	37	33
COF-316	557	12	11
COF-318	576	15	11
COF-C	330	14	34
COF-O	477	15	34
CS-COF	776	16	7
DBOV-COF	581	19	35
TP-COF	868	31.4	36
DPP2-HHTP-COF	1000	33	37
FL-COF-1	1308	21	25
HP-FAN	56.5	11.6	28
JUC-505	1584	1.6.8	12
JUC-506	1655	28.4	12
PPy-COF	923	18.8	38
TANG-COF	440	31	26
TPB-TFB COF	1320	17	39
TTO-COF	390.35	12.3	40
sp^{2}c-COF-4	369	32	41
PTZ–TTA-COF	740	19	42

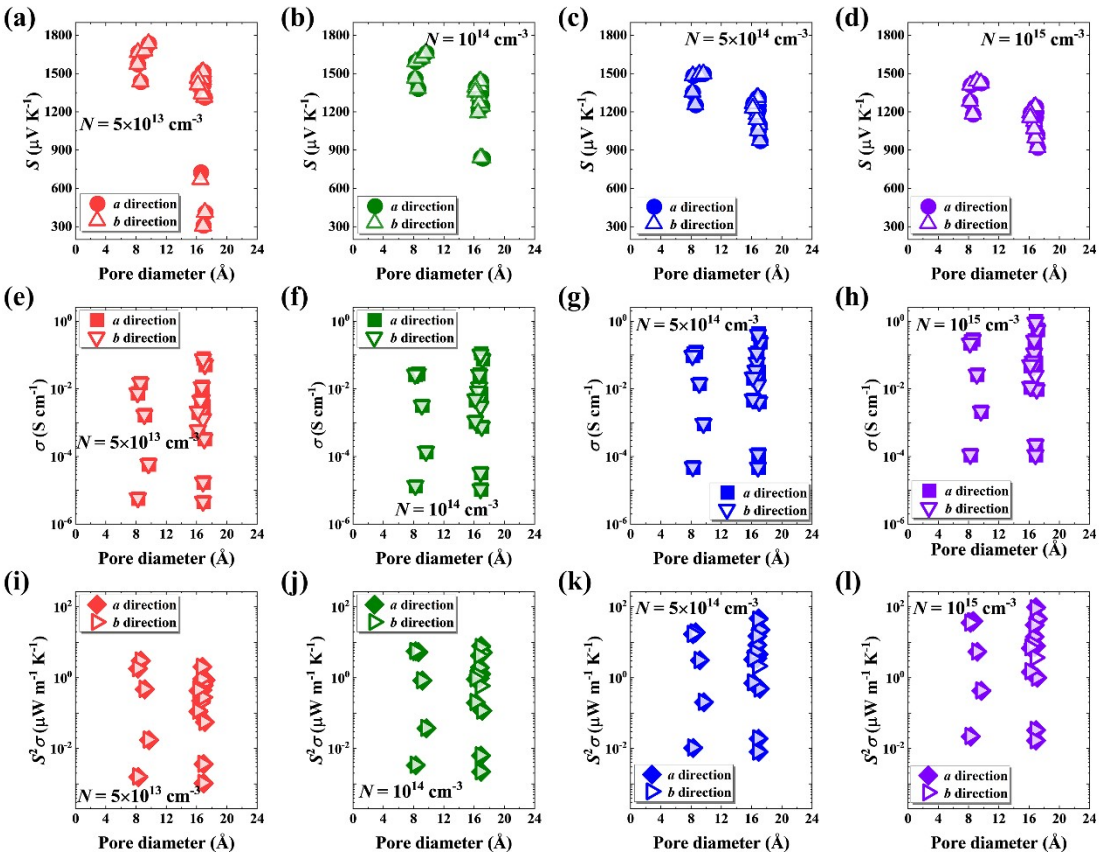

Fig. S11 The correlation between our calculated room-temperature (**a**–**d**) Seebeck coefficients (S), (**e**–**h**) conductivity (σ), (**i**–**l**) power factor ($S^2\sigma$) and pore diameters for our studied 17 two-dimensional COFs.

Section 6. Implications for other classes of COFs

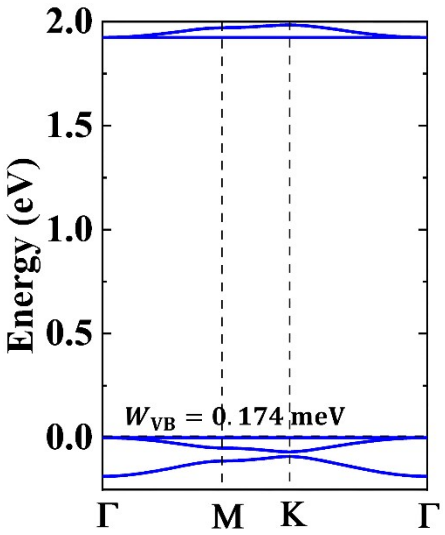

Fig. S12 Calculated band structure of FL-COF-1[25]. The valence band width (W_{VB}) is displayed in the figure. The Fermi energy levels are displayed in black horizontal dashed lines. The reciprocal coordinates of high symmetry *k*-points in the first Brillouin zone are Γ = (0, 0, 0), M = (1/2, 0, 0), and K = (1/3, 1/3, 0).

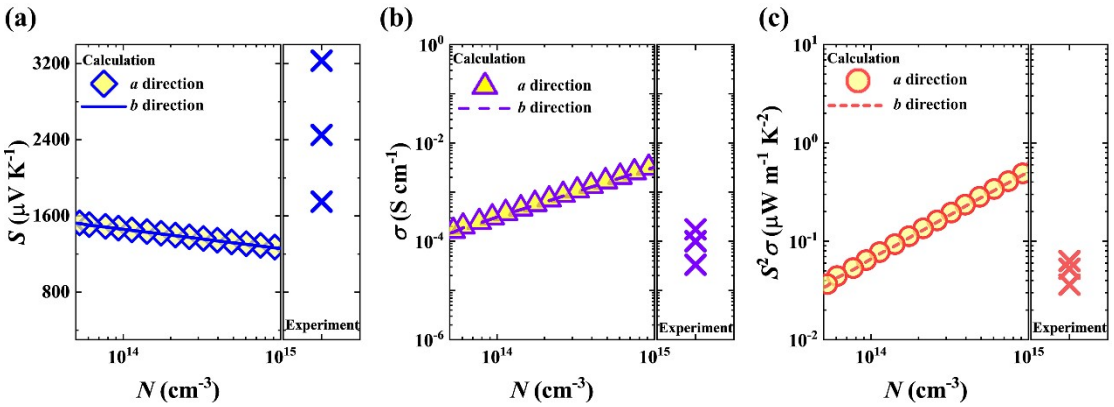

Fig. S13 Comparison of the calculated room-temperature (**a**) Seebeck coefficient (S), (**b**) conductivity (σ), and (**c**) power factor ($S^2\sigma$), and the measured results for FL-COF-1.

Table S13. Seebeck coefficient (S), conductivity (σ), and power factor ($S^2\sigma$) for FL-COF-1 along the *a* and *b* directions at the hole concentration (N) of around 5×10^{13}, 10^{14}, 5×10^{14}, and 10^{15} cm^{-3}, respectively at room temperature.

	N (cm^{-3})	S ($\mu V\ K^{-1}$)		σ ($S\ cm^{-1}$)		$S^2\sigma$ ($\mu W\ m^{-1}\ K^{-2}$)	
		a	*b*	*a*	*b*	*a*	*b*
FL-COF-1	5.30×10^{13}	1.52×10^{3}	1.52×10^{3}	1.56×10^{-4}	1.54×10^{-4}	0.0360	0.0355
	1.14×10^{14}	1.45×10^{3}	1.45×10^{3}	3.64×10^{-4}	3.59×10^{-4}	0.0762	0.0751
	4.94×10^{14}	1.32×10^{3}	1.32×10^{3}	1.61×10^{-3}	1.58×10^{-3}	0.279	0.275
	1.15×10^{15}	1.25×10^{3}	1.25×10^{3}	3.75×10^{-3}	3.69×10^{-3}	0.582	0.573

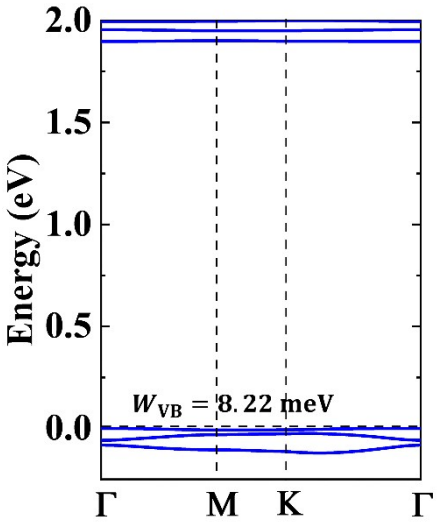

Fig. S14 Calculated band structure of the hexagonal sp^{2}c-COF-4[41]. The valence band width (W_{VB}) is displayed in the figure. The Fermi energy levels are displayed in black horizontal dashed lines. The reciprocal coordinates of high symmetry *k*-points in the first Brillouin zone are Γ = (0, 0, 0), M = (1/2, 0, 0), and K = (1/3, 1/3, 0).

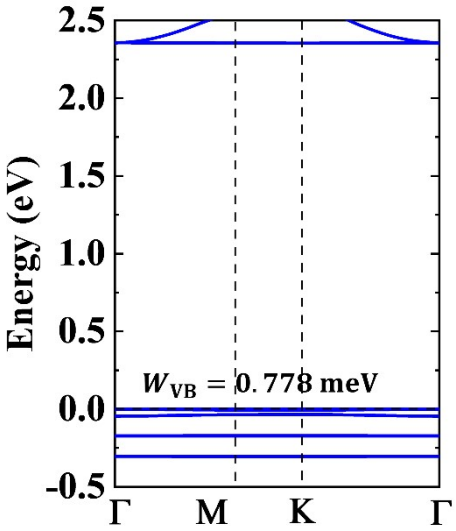

Fig. S15 Calculated band structure of the TTO-COF[40]. The valence band width (W_{VB}) is displayed in the figure. The Fermi energy levels are displayed in black horizontal dashed lines. The reciprocal coordinates of high symmetry *k*-points in the first Brillouin zone are Γ = (0, 0, 0), M = (1/2, 0, 0), and K = (1/3, 1/3, 0).

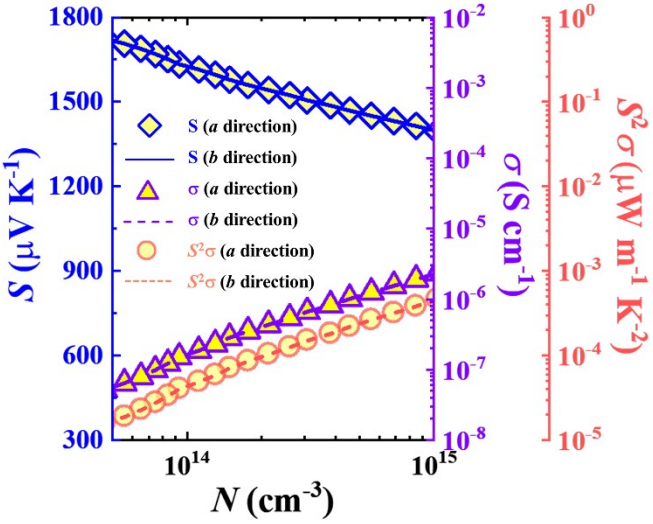

Fig. S16 Seebeck coefficient (S), conductivity (σ), and power factor ($S^2\sigma$) of TTO-COF along the *a* and *b* directions, respectively at the hole concentration from 5×10^{13} cm^{-3} to 1×10^{15} cm^{-3} at room temperature. The Seebeck coefficients are displayed in blue diamond and blue solid line along the *a* and *b* directions, respectively. The conductivities are displayed in purple triangle and purple dashed line along the *a* and *b* directions, respectively. The power factors are displayed in oranges circle and orange short dashed line along the *a* and *b* directions, respectively.

Table S14. Seebeck coefficient (S), conductivity (σ), and power factor ($S^2\sigma$) for TTO-COF along the *a* and *b* directions at the hole concentration (N) of around 5×10^{13}, 10^{14}, 5×10^{14}, and 10^{15} cm^{-3}, respectively at room temperature.

	N (cm^{-3})	S ($\mu V\ K^{-1}$)		σ ($S\ cm^{-1}$)		$S^2\sigma$ ($\mu W\ m^{-1}\ K^{-2}$)	
		a	*b*	*a*	*b*	*a*	*b*
TTO-COF	5.58×10^{13}	1.71×10^{3}	1.71×10^{3}	6.43×10^{-8}	6.19×10^{-8}	1.87×10^{-5}	1.80×10^{-5}
	1.12×10^{14}	1.61×10^{3}	1.62×10^{3}	1.86×10^{-7}	1.79×10^{-7}	4.84×10^{-5}	4.66×10^{-5}
	5.58×10^{14}	1.45×10^{3}	1.45×10^{3}	1.25×10^{-6}	1.20×10^{-6}	2.63×10^{-4}	2.53×10^{-4}
	1.03×10^{15}	1.40×10^{3}	1.40×10^{3}	2.36×10^{-6}	2.27×10^{-6}	4.60×10^{-4}	4.43×10^{-4}

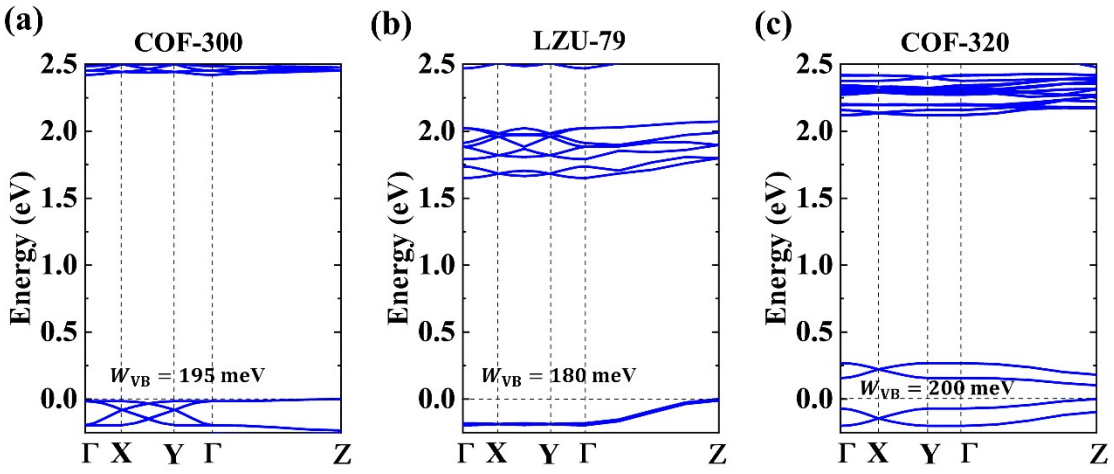

Fig. S17 Calculated band structures of (**a**) COF-300[43], (**b**) LZU-79[43], and (**c**) COF-320[44]. The valence band width (W_{VB}) is displayed in the figure. The Fermi energy levels are displayed in black horizontal dashed lines. The reciprocal coordinates of high symmetry *k*-points in the first Brillouin zone are Γ = (0, 0, 0), X = (1/2, 0, 0), Y = (0, 1/2, 0), and Z = (0, 0, 1/2).

Section 7. Supporting reference

1 P. E. Blochl, *Phys. Rev., B Condens. Matter.*, 1994, **50**, 17953-17979.
2 J. P. Perdew, K. Burke and M. Ernzerhof, *Phys. Rev. Lett.*, 1996, **77**, 3865-3868.
3 S. Grimme, J. Antony, S. Ehrlich and H. Krieg, *J. Chem. Phys.*, 2010, **132**, 154104.
4 G. Kresse and J. Furthmüller, *Comput. Mater. Sci.*, 1996, **6**, 15-50.
5 Z. Tian, V. S. Kale, Y. Wang, S. Kandambeth, J. Czaban-Jozwiak, O. Shekhah, M.

Eddaoudi and H. N. Alshareef, *J. Am. Chem. Soc.*, 2021, **143**, 19178-19186.
6 Y. Jiang, H. Jung, S. H. Joo, Q. K. Sun, C. Li, H. J. Noh, I. Oh, Y. J. Kim, S. K. Kwak, J. W. Yoo and J. B. Baek, *Angew. Chem. Int. Ed. Engl.*, 2021, **60**, 17191-17197.
7 J. Guo, Y. Xu, S. Jin, L. Chen, T. Kaji, Y. Honsho, M. A. Addicoat, J. Kim, A. Saeki, H. Ihee, S. Seki, S. Irle, M. Hiramoto, J. Gao and D. Jiang, *Nat. Commun.*, 2013, **4**, 2736.
8 S. Jhulki, J. Kim, I.-C. Hwang, G. Haider, J. Park, J. Y. Park, Y. Lee, W. Hwang, A. A. Dar, B. Dhara, S. H. Lee, J. Kim, J. Y. Koo, M. H. Jo, C.-C. Hwang, Y. H. Jung, Y. Park, M. Kataria, Y.-F. Chen, S.-H. Jhi, M.-H. Baik, K. Baek and K. Kim, *Chem.*, 2020, **6**, 2035-2045.
9 J. Mahmood, E. K. Lee, H. J. Noh, I. Ahmad, J. M. Seo, Y. K. Im, J. P. Jeon, S. J. Kim, J. H. Oh and J. B. Baek, *Adv. Mater.*, 2021, **33**, e2004707.
10 J. Mahmood, E. K. Lee, M. Jung, D. Shin, I. Y. Jeon, S. M. Jung, H. J. Choi, J. M. Seo, S. Y. Bae, S. D. Sohn, N. Park, J. H. Oh, H. J. Shin and J. B. Baek, *Nat. Commun.*, 2015, **6**, 6486.
11 B. Zhang, M. Wei, H. Mao, X. Pei, S. A. Alshmimri, J. A. Reimer and O. M. Yaghi, *J. Am. Chem. Soc.*, 2018, **140**, 12715-12719.
12 X. Guan, H. Li, Y. Ma, M. Xue, Q. Fang, Y. Yan, V. Valtchev and S. Qiu, *Nat. Chem.*, 2019, **11**, 587-594.
13 S. Chen, Y. Wu, Y. Zhang, W. Zhang, Y. Fu, W. Huang, T. Yan and H. Ma, *J. Mater. Chem. A*, 2020, **8**, 13702-13709.
14 X. Guo, T. Zheng, G. Ji, N. Hu, C. Xu and Y. Zhang, *J. Mater. Chem. A*, 2018, **6**, 10243-10252.
15 W. Shi, G. Wu, X. Yong, T. Deng, J. S. Wang, J. C. Zheng, J. Xu, M. B. Sullivan and S. W. Yang, *ACS Appl. Mater. Interfaces*, 2018, **10**, 35306-35315.
16 M. Wang, M. Ballabio, M. Wang, H. H. Lin, B. P. Biswal, X. Han, S. Paasch, E. Brunner, P. Liu, M. Chen, M. Bonn, T. Heine, S. Zhou, E. Canovas, R. Dong and X. Feng, *J. Am. Chem. Soc.*, 2019, **141**, 16810-16816.
17 M. Wang, M. Wang, H. H. Lin, M. Ballabio, H. Zhong, M. Bonn, S. Zhou, T. Heine, E. Canovas, R. Dong and X. Feng, *J. Am. Chem. Soc.*, 2020, **142**, 21622-21627.
18 Y. Yue, P. Cai, X. Xu, H. Li, H. Chen, H. C. Zhou and N. Huang, *Angew. Chem. Int. Ed. Engl.*, 2021, **60**, 10806-10813.
19 L. Wang, C. Zeng, H. Xu, P. Yin, D. Chen, J. Deng, M. Li, N. Zheng, C. Gu and Y. Ma, *Chem. Sci.*, 2019, **10**, 1023-1028.
20 H. Duan, P. Lyu, J. Liu, Y. Zhao and Y. Xu, *ACS Nano*, 2019, **13**, 2473-2480.
21 E. Jin, K. Geng, S. Fu, S. Yang, N. Kanlayakan, M. A. Addicoat, N. Kungwan, J. Geurs, H. Xu, M. Bonn, H. I. Wang, J. Smet, T. Kowalczyk and D. Jiang, *Chem.*, 2021, **7**, 3309-3324.
22 S. Wang, L. Da, J. Hao, J. Li, M. Wang, Y. Huang, Z. Li, Z. Liu and D. Cao, *Angew. Chem. Int. Ed. Engl.*, 2021, **60**, 9321-9325.
23 S. Wang, X. X. Li, L. Da, Y. Wang, Z. Xiang, W. Wang, Y. B. Zhang and D. Cao, *J. Am. Chem. Soc.*, 2021, **143**, 15562-15566.
24 S. Ghosh, Y. Tsutsui, T. Kawaguchi, W. Matsuda, S. Nagano, K. Suzuki, H. Kaji

and S. Seki, *Chem. Mater.*, 2022, **34**, 736-745.
25 L. Wang, B. Dong, R. Ge, F. Jiang and J. Xu, *ACS Appl. Mater. Interfaces*, 2017, **9**, 7108-7114.
26 V. Lakshmi, C.-H. Liu, M. Rajeswara Rao, Y. Chen, Y. Fang, A. Dadvand, E. Hamzehpoor, Y. Sakai-Otsuka, R. S. Stein and D. F. Perepichka, *J. Am. Chem. Soc.*, 2020, **142**, 2155-2160.
27 J. M. Rotter, R. Guntermann, M. Auth, A. Mahringer, A. Sperlich, V. Dyakonov, D. D. Medina and T. Bein, *Chem. Sci.*, 2020, **11**, 12843-12853.
28 H.-J. Noh, S. Chung, M. S. Okyay, Y.-K. Im, S.-W. Kim, D.-H. Kweon, J.-P. Jeon, J.-M. Seo, N.-H. Kim, S.-Y. Yu, Y. Reo, Y.-Y. Noh, B. Kang, N. Park, J. Mahmood, K. Cho and J.-B. Baek, *Chem.*, 2022, **8**, 3130-3144.
29 X. Feng, L. Chen, Y. Honsho, O. Saengsawang, L. Liu, L. Wang, A. Saeki, S. Irle, S. Seki, Y. Dong and D. Jiang, *Adv. Mater.*, 2012, **24**, 3026-3031.
30 Z. Li, X. Feng, Y. Zou, Y. Zhang, H. Xia, X. Liu and Y. Mu, *Chem. Commun. (Camb)*, 2014, **50**, 13825-13828.
31 A. Nagai, Z. Guo, X. Feng, S. Jin, X. Chen, X. Ding and D. Jiang, *Nat. Commun.*, 2011, **2**, 536.
32 E. L. Spitler, B. T. Koo, J. L. Novotney, J. W. Colson, F. J. Uribe-Romo, G. D. Gutierrez, P. Clancy and W. R. Dichtel, *J. Am. Chem. Soc.*, 2011, **133**, 19416-19421.
33 T. Sick, J. M. Rotter, S. Reuter, S. Kandambeth, N. N. Bach, M. Doblinger, J. Merz, T. Clark, T. B. Marder, T. Bein and D. D. Medina, *J. Am. Chem. Soc.*, 2019, **141**, 12570-12581.
34 F. Yu, W. Liu, B. Li, D. Tian, J. L. Zuo and Q. Zhang, *Angew. Chem. Int. Ed. Engl.*, 2019, **58**, 16101-16104.
35 E. Jin, S. Fu, H. Hanayama, M. A. Addicoat, W. Wei, Q. Chen, R. Graf, K. Landfester, M. Bonn, K. A. I. Zhang, H. I. Wang, K. Mullen and A. Narita, *Angew. Chem. Int. Ed. Engl.*, 2022, **61**, e202114059.
36 S. Wan, J. Guo, J. Kim, H. Ihee and D. Jiang, *Angew. Chem. Int. Ed. Engl.*, 2008, **47**, 8826-8830.
37 S. Rager, A. C. Jakowetz, B. Gole, F. Beuerle, D. D. Medina and T. Bein, *Chem. Mater.*, 2019, **31**, 2707-2712.
38 S. Wan, J. Guo, J. Kim, H. Ihee and D. Jiang, *Angew. Chem. Int. Ed. Engl.*, 2009, **48**, 5439-5442.
39 S. Fu, E. Jin, H. Hanayama, W. Zheng, H. Zhang, L. Di Virgilio, M. A. Addicoat, M. Mezger, A. Narita, M. Bonn, K. Mullen and H. I. Wang, *J. Am. Chem. Soc.*, 2022, **144**, 7489-7496.
40 Y. Yang, H. Niu, L. Xu, H. Zhang and Y. Cai, *Appl. Catal. B*, 2020, **269**.
41 E. Jin, K. Geng, K. H. Lee, W. Jiang, J. Li, Q. Jiang, S. Irle and D. Jiang, *Angew. Chem. Int. Ed. Engl.*, 2020, **59**, 12162-12169.
42 Y. Liu, X. Jiang, L. Chen, Y. Cui, Q.-Y. Li, X. Zhao, X. Han, Y.-C. Zheng and X.-J. Wang, *J. Mater. Chem. A*, 2023, **11**, 1208-1215.
43 T. Ma, E. A. Kapustin, S. X. Yin, L. Liang, Z. Zhou, J. Niu, L. H. Li, Y. Wang, J. Su, J. Li, X. Wang, W. D. Wang, W. Wang, J. Sun and O. M. Yaghi, *Science*, 2018, **361**, 48-52.

44 Y. B. Zhang, J. Su, H. Furukawa, Y. Yun, F. Gandara, A. Duong, X. Zou and O. M. Yaghi, *J. Am. Chem. Soc.*, 2013, **135**, 16336-16339.